Segmented Deformable Mirrors for Ground Layer Adaptive Optics

Edward Kibblewhite
University of Chicago, Adaptive Photonics LLC

ABSTRACT

Current designs of monolithic deformable secondary mirrors use a dense actuator spacing, both to achieve adequate fitting error and damping to the thin faceplate. Ground layer AO can be effective with less actuators but damping may become more of a problem. A highly segmented architecture for the deformable secondary should be able to achieve good GLAO performance with less cost and complexity, especially for the next generation telescopes.
This paper discusses the design of one such mirror optimized for a 12-meter class telescope. It is shown that the forces required to control the segments should be ≈ 0.02N/actuator and that the electronics can be integrated into the segment itself. Total power requirements of less than 100 watts/m^2, with a total weight of less than 100 kg/m^2 appear possible. The technology is directly scalable to the large DSMs required by ELTs.
The use of single LGS beacons for wide field AO is also discussed. It is suggested that a single Rayleigh beacon can reduce the FWHM by a factor of over 2 over a 5 arc-minute field of view for a 12 m telescope at a site similar to Mauna Kea. A factor of 5 reduction may be possible over a 1 arc-minute field of view using a sodium beacon.

Keywords: Adaptive Optics, Deformable Secondary Mirrors, Segmented Mirrors, Ground Layer Adaptive Optics, Laser Guide Stars.

1. INTRODUCTION

The effectiveness of GLAO depends on the site. It appears to be of most benefit at Mauna Kea and may be significantly less at other sites. In any case the seeing improvement is not large, being at best a factor of ≈ 2 in FWHM and is typically less than 1.5. However, only a modest number of degrees of freedom appear to be needed for good correction for GLAO. Figure 1 shows the FWHM as a function of number of actuators calculated for the 8m Gemini telescope [1]

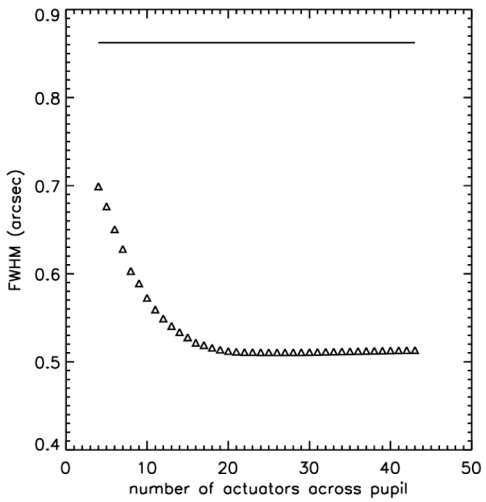

Figure 1: Calculated FWHM for GLAO correction as a function of number of actuators for 8 m Gemini telescope.

The Gemini study showed that 95% of the optimum performance would be recovered with about 300 degrees of freedom at the DM. The wide field of view that is available by GLAO requires either a deformable secondary or primary mirror to provide the wavefront correction. The current generation of DSMs all use a thin monolithic faceplate to define the optical surface [2] [3]. This faceplate floats above a reference plate and whose surface is controlled by an array of force actuators. Because the faceplate has a low fundamental frequency and a high Q, a combination of both active and passive (air film) damping of the faceplate is required to provide stability. This has driven the technical design of the

DSM towards an actuator spacing of ≈ 0.03 m and a faceplate thickness of ≈0.002 m. Doubling the actuator spacing would result in significant changes to the design and has not yet been demonstrated on the sky. While conventional AO is used on most large telescopes today, the modest improvement to the PSF, coupled with the high cost and complexity of the current technology, has limited the introduction of GLAO into astronomy. Scaling current DSM technology to the larger sizes required by ELT projects also poses other engineering problems. The weight of the DSM scales very approximately as D^3 and monolithic faceplates become increasingly fragile as the diameter increases.

2. BASIC CONCEPT

The basic concept described in this paper is to build the DSM from a number of small segments equipped with independent actuators and position control systems. In this design, there is no reference plate to define the position of the faceplate surface, rather the actuators are supported on a lightweight and somewhat compliant backing structure with their relative positions being determined by edge sensors. This is a similar concept to that used for the primary mirror of Keck, and the design of TMT and the E-ELT. Each segment requires 3 actuators to control its position. This number is offset by the potentially better fitting error of the segment. Simulations show that segment diameters of between 1.4 and 1.7 of conventional DM actuator spacing have similar fitting errors, the numerical factor depending on the shape and edge conditions of the segments. For an 8 m telescope we would therefore need 160 segments of approximately 0.09 m diameter to attain the 95% level of performance indicated in figure 1. The size and design of each segment is approximately independent of the diameter of the primary mirror, but the number of segments will increase with f its area.

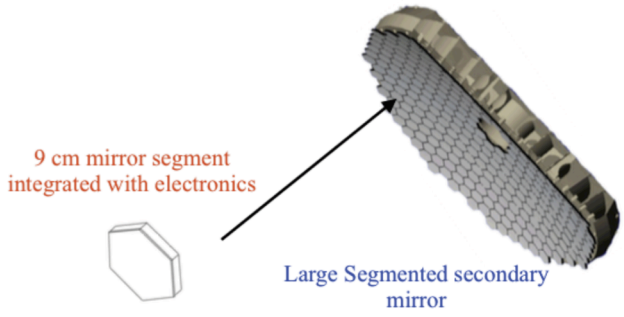

Figure 2: Schematic diagram showing the segment arrangement for a large segmented deformable secondary mirror.

The advantages of this approach are:

(1) *The actuator spacing depends on the performance required by the GLAO system rather than the requirement to damp out high frequency resonances within the faceplate.* This reduces the number actuators needed to meet the needs of GLAO and reduces the cost, complexity and power requirements of the DSM.

(2) *The total power/segment should be in the region of ½ to 1 watt.* This is achieved because the power required to drive the segments is low and edge sensors have been recently developed operating with powers of a few tens of mW. A 1.2 m DSM suitable for GLAO should only dissipate ≈ 100 watts of heat.

(3) *The weight of the DSM assembly is significantly reduced.* The weight of the assembly is expected to be less than 100 kg/m^2, excluding the weight of a hexapod. The DSM will be lighter than even a light-weighted monolithic secondary mirror.

(4) *The technology is scalable to large diameters*. The technology allows construction of a DSM for TMT.

(5) *Mirror production is straightforward*. A number of different vendors are equipped to polish the surface of the segments in large numbers and economic cost. A small set of test plates can be provided to ensure economic and reliable testing of the segment surface. Table 1 gives the worst case Zernike term for coma and astigmatism for a 0.09 m segments size, for a different telescopes.

TABLE 1 (Zernike terms for segment at the edge of the pupil)

Zernike term	Keck telescope	F 1.6 12 m telescope	TMT
C22	-4.05 μm	-4.55 μm	-6.54 μm
C31	0.203 μm	0.195 μm	0.097 μm

(6) High reflectivity, uniform multilayer coatings can be easily applied to the small segments. This reduces the emissivity of the DSM.

(7) Segments can be replaced in the field. Each segment contains its own electronics and actuators as self-contained unit.

The major disadvantages are:

(1) *The space between the segments increases the emissivity of the mirror*. This effect will increase the emissivity by 0.5% for a spacing of 250 μm between typical segment sizes. However, the DSM can incorporate an aperture in the center of similar size to the secondary mirror, observed at the exit pupil of the telescope and reducing the thermal background of the telescope. The small size of the segments allows deposition of high reflectivity coatings to be laid down at relatively low cost. In practice, the overall emissivity of the mirror should be substantially lower than monolithic DSMs.

(2) *The segment edges will increase the scattered light*. The fraction of scattered light will be less than that caused by the primary mirror. For GLAO applications, the strongest satellite images will be within the psf core.

(3) *Simultaneous calibration of highly segmented primary and secondary mirrors using on sky wavefront sensors*. It is probable that on-sky wavefront sensors will be needed to calibrate the edge sensors for both primary and secondary mirrors to track long-term drifts. While a Gregorian DSM can be independently calibrated using its own laser reference source, this is more difficult with the RC optical design of TMT and the E-ELT. Although it may also put additional constraints on the large term stability of edge sensors, the technical difficulty of solving this problem is likely to be similar for both monolithic and highly segmented mirror DMs. It is under active study by a number of different groups.

(3) FORCES REQUIRED TO MOVE SEGEMENTS

3.1 Tracking Atmospheric Turbulence

Atmospheric turbulence moves a point on the wavefront typically by 1 radian in a time scale of 0.81 r_0/v, where r_0 is the Fried parameter at a given wavelength and v is a typical wind speed [4]. This implies that the mean velocity of any part of the wavefront will be around 10^{-5} m/s with accelerations of order 10^{-3} m/s^2. In practice, the finite size of the segment attenuates the power spectrum at high spatial frequencies, so that the required acceleration of a segment to follow the distorted wavefront is substantially reduced.

If we assume that positions of all the segments are measured from the central segment, rather than a minimum norm solution (a worst case assumption), we can use the relevant Power Spectrum given in [5] and write the mean square acceleration of a given segment as:

$$\Phi_a(f) = \frac{31.5\nu^4}{V}\int_0^\infty \left(\frac{Sin[\pi b\sqrt{(\nu/V)^2 + f^2 + f_0^2}\,]J_1[\pi d\sqrt{(\nu/V)^2 + f^2 + f_0^2}\,]}{\pi d\sqrt{(\nu/V)^2 + f^2 + f_0^2}} \right)^2 \left((\nu/V)^2 + f^2 + f_0^2\right)^{-11/6} df$$

Where: ν is the frequency in Hz.
V is the wind speed.
b is the radial distance of the segment from the optical axis.
d is the effective diameter of the segment.
f_0 is related to the outer scale length.

The mean square acceleration is given by integrating this equation for all frequencies.

Only small forces are required to produce these accelerations. For example, if the segment size is 0.65 m and the distance to the optical axis is 15 m, we obtain an rms acceleration of 0.50 mm/sec^2 for a wind speed of 10 m/sec and an r_0 of 0.1m at 0.5 µm. This corresponds to an rms pressure over the secondary of about 0.008 Pa for a segment mass density of 15 kg/m^2.

3.2 Compensating wind forces

Wind forces are more significant than the effects of atmospheric turbulence. The normalized power spectrum of wind forces is given by [6]:

$$\Phi_w(f) = \frac{0.7731/f_0}{\left(1+(f/f_0)^2\right)^{7/6}}$$

Where: $f_0 = 0.2$ V/d.

MacMynowski [7] suggests that the wind speed at the secondary mirror is ¼ the wind speed at the site. Under these conditions, the power spectrum due to wind and reaction forces tracking the atmospheric wavefront are shown in figure 3 for a wind speed at the site of 15 m/s. The rms force due to wind buffeting at the secondary mirror is 3.8 Pa.

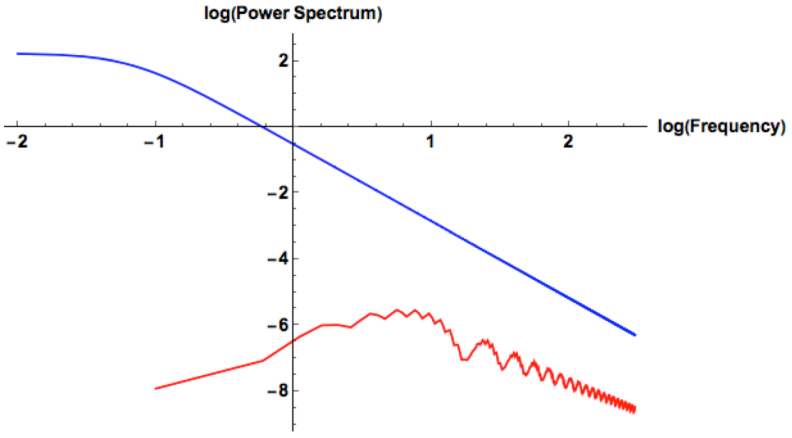

Figure 3: Power spectrum of pressure at secondary due to wind buffeting (upper, blue) and reaction forces required to track atmospheric turbulence (lower, red). Outside wind speed is 10 m/s, Fried parameter = 0.1 m @ 0.5 µm. Calculation for a 30 m telescope, segment size at entrance pupil 0.65 m located at the edge of the pupil. Units are Pa^2/Hz and Hz.

3.3 Actuator forces

The weight of the segment will be supported using an additional servo loop to drive the dc current to the actuators to zero and correct for changes in azithumal position (see below) . However, in practice, additional forces from the actuators may be needed to correct for residual astatic displacements. Assuming that the outer servo loop only removes 95% of the gravitational force and that the weight of each segment (including integrated electronics) is 0.1 kg, the rms force required to stabilize a segment size of 9 cm effective diameter will still only be of order ≈ 0.02 N/actuator and could be a factor of 2 lower. This compares with rms forces of 0.16 N/actuator required for the ESO DSM [8].

4. DESIGN OF SEGMENT

The conceptual design of the segment is shown in figure 4. A SiC or lightweighted Zerodur plate is supported in the center by an actuator taking out large-scale offsets and is connected to 2 sets of 3 actuators. Three of these actuators provide the high frequency drive capability and the other three are passive devices, used to damp out high frequency vibrations within the structure. Although adequate damping may be possible using only the control actuators, passive damping of the DSM has proved crucial for both conventional DSM and earlier NASA program to develop segmented mirror technology [9].

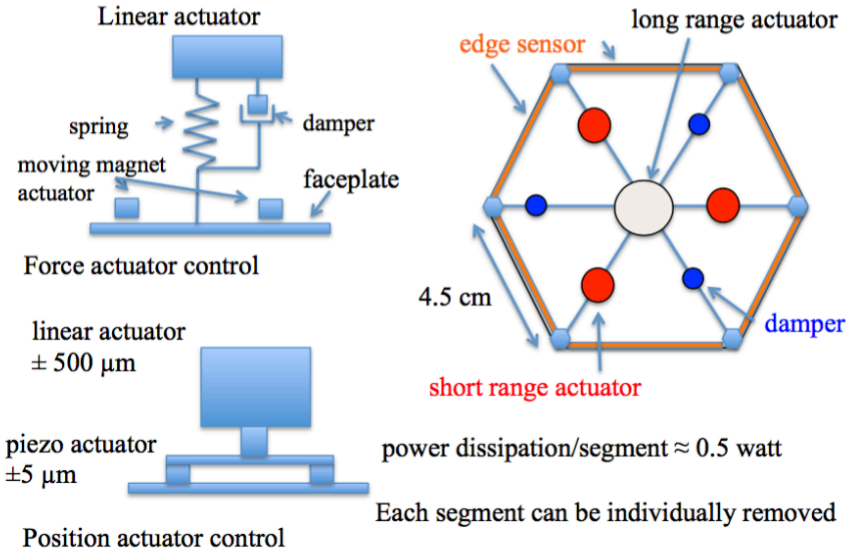

Figure 4: Hierarchical Control of a segment using force or position actuators

4.1 Interaction between Segments

To save weight, the fundamental resonant frequency of the backing structure may be << that of the control loop. Under this condition, a step change in the position of one actuator can potentially influence the position of its neighbors and, in the worst case, cause instability of the whole DSM. This situation has been modeled for a much larger system, based on the design of a 25 m ELT using an adaptive primary mirror [10]. In this design, the backing structure had a fundamental resonance frequency of ≈ 15 Hz., the segments were 0.3 m on side and weighed 3 kg. This model showed that the displacement of one segment by 1 µm introduced a 15 nm displacement in its neighbors, which was quickly damped. Although the fundamental frequency of the backing plate is low, its resonate frequencies on spatial scales similar to the segment spacing is still high. Transmission of energy to segments at longer spatial scales is damped, both by the backing structure and the segment control systems. This effect will be lower for the segments DSM, both because of the lower mass of the segments and the higher fundamental resonant frequency of the backing structure.

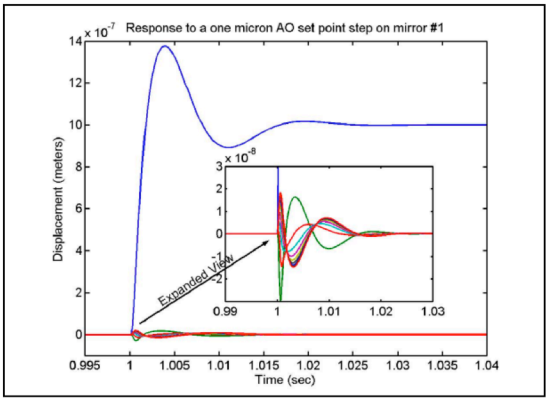

Figure 5: Displacement of a 3 kg primary mirror segment from the ATLAS project by 1 µm together with displacements of neighboring segments on a compliant backing structure. [11]

4.2 Edge sensors

The development of suitable edge sensors presents perhaps the biggest technical challenge. Not only must these sensors have low noise and high bandwidth but they must also be compact, lightweight and operate at low power. An inductive sensor originally developed for the ATLAS project has been modified to provide accuracies of < 0.1 nm/√Hz with an update rate of $> 10^5$ kHz and a linear range of ± 150 µm. The coils are currently fabricated on a substrate of G4. We expect to reduce the power requirements of each sensor to less than 50 mW and to fabricate the coils onto a low expansion material.

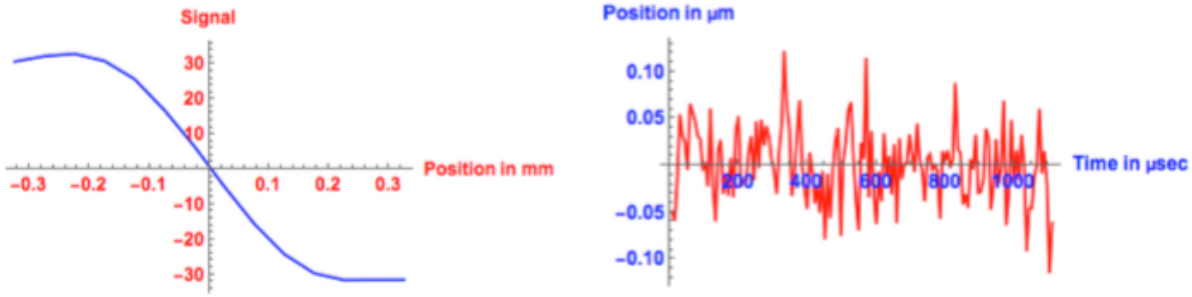

Figure 6: Output of prototype inductive sensor electronics as a function of position (left). Position noise of a sensor is shown on the right. Update time is 7 µsec.

5. LASER GUIDE STAR REQUIREMENTS FOR GLAO

5.1 Ideal LGD constellation

GLAO requires a suitable DSM, the deployment of an adequate laser guide star constellation, and a complex control system. This is difficult to model. However, an ideal GLAO wavefront sensor would use a dense packed ring of stars around the edge of the field of view [12]. This provides not only the best correction across the field of view but has an analytic solution for the structure function given by:

$$D[r] = \sum_{i=N_{layers}} 6.145 r_0^{-5/3}(h_i) \int_{0.5/d_s}^{\infty} (1 - J_o[\kappa r])(1 - J_0[\kappa \beta_0 h_i])^2 \, d\kappa$$

Where: $r_0\,(h_i)$ is the appropriate value of r_0 for a layer at height h above the site.
β_0 is the radius of the dense packed ring of stars.

This analysis enables use to compare the performance of practical WFS schemes with the theoretical best model, which assumes high SNR and bandwidth for the AO system. If we assume that the telescope has a diameter of 12 m and is located at a site with a similar C_N^2 profile as Mauna Kea [13] we can calculate the 50% energy radius relative to the uncorrected seeing as a function of spacing between actuators and field of view. This is shown in figure 7:

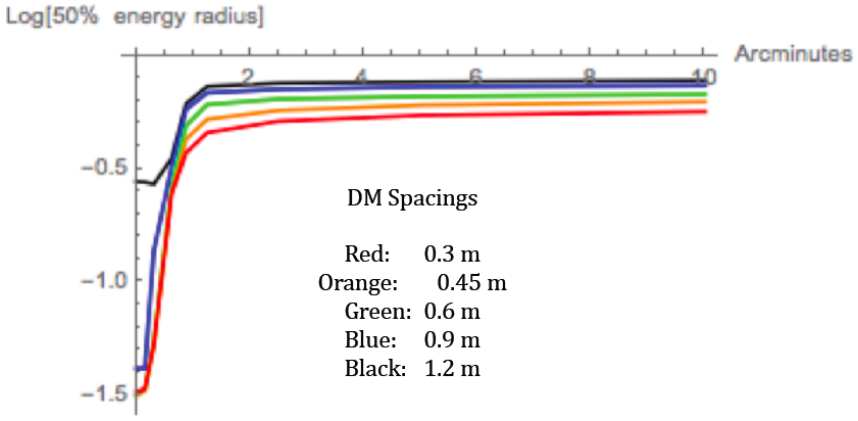

Figure 7: Log_{10} of radius containing 50% of the energy for a GLAO corrected psf relative to uncorrected psf as a function of field radius in arcminutes. A value of -1.0 corresponds to a psf 1/10 of the uncorrected psf. DM actuator spacings are for an idealized hexagonal grid. A segmented mirror of diameter 1.5 to 1.7 times this spacing would have similar performance.

When realistic wavefront sensor noise and finite servo bandwidth are included in the model there is a broad optimum in performance for an hexagonal actuator spacing in the range of 0.3 to 0.45 m. This agrees with the Gemini analysis [1]. Conventional GLAO is thus seen to be able to provide modest correction at wide (≥ 30 arcminute) radii, but note that the figure also shows much better correction round the central field of around 1 arcminute diameter. We can operate the AO system in this mode - the geometry of the guide stars is still a ring but its radius has been greatly reduced.

5.2 Use of Rayleigh Beacon for large telescopes

A single low altitude laser beacon operated on 8 to 12 m telescope can also provide good performance over a significantly large field of view at potentially lower cost and complexity. The low altitude beacon measures the ground layer with high accuracy and higher layers with much less accuracy and it is unable to measure any turbulence above the beacon. The cone effect also spreads out the turbulence over a small area of the high altitude layer across a larger area in the pupil at the telescope. It is more difficult to calculate the point spread function across the field of view because the change of scale of wavefront as a function of height does not allow a straightforward analytic solution in the Fourier domain. Tokovinin [12] gives an approximate equation for calculating the structure function of an on-axis point source corrected using a single laser beacon:

$$D[r_i] = 6.145 r_0(i)^{-5/3} \int_0^{\infty} \left(1 - J_0[\kappa r]\right) \cdot \kappa \left(\kappa^2 + \left(2\pi / L_0\right)^2\right)^{-11/6}$$
$$\cdot \left(1 - R(\kappa) 2\gamma \left(4 J_1\left[0.5\kappa d_{tel} h_i / h_{laser}\right] / \left(\kappa d_{tel} h_i / h_{laser}\right)\right) + \gamma^2 R(\kappa)^2\right) \cdot d\kappa$$

Where: $D\,[r_i]$ is the structure function of the *ith* layer with a Fried parameter of $r_0(i)$.
$R(\kappa)$ is the DM filter function which, in this model, is 1 for frequencies less than $k<\pi/d_s$ and 0 otherwise.

The first order Bessel term averages the power spectrum over the pupil and the γ term represents a geometric effect due to the finite range of the laser guide star given by:

$$\gamma = 1 - h_i / h_{laser}$$

Figure 9 shows the variation of PSF as a function of field angle using the approach of Sasiela [13] to calculate the mean square error of the wavefront across the pupil as a function of beacon height and angular distance from the target. In this case we have calculated an effective r_0, which is defined as the r_0 of the atmosphere that would give the same mean square wavefront error for a tilt removed wavefront.

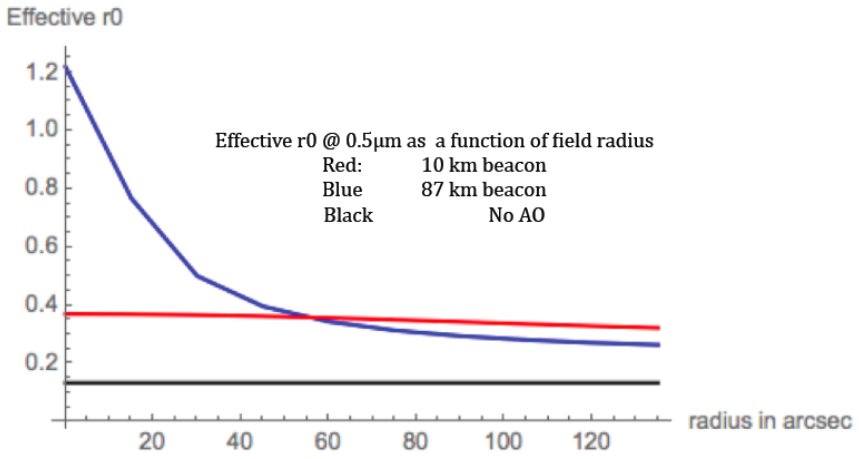

Figure 9: Effective r_0 as a function of field angle for images corrected by a Sodium beacon (height 87 km) and Rayleigh beacon (height 10 km). The values of effective r_0 are given at a wavelength of 0.5 μm. Calculations are for a 12 m telescope operated in similar median seeing conditions to Mauna Kea

This figure shows that a single low altitude Rayleigh beacon can provide good GLAO correction over a wide field of view (at least 5 arcminutes), and that a single sodium beacon can provide even better correction (but not diffraction limited) over a smaller area. A single sodium beacon could provide an improvement of a factor of >5 in effective r_0 over a smaller area, resulting in observations for point sources of <1/25 of the time.

6. CONCLUSIONS

It should be possible to fabricate small, "smart", segments, equipped with a significant fraction of its electronics located within the structure, as building blocks for large DSMs. These DSMs would be significantly lighter, cheaper and lower power compared to current monolithic technology. Once this technology is demonstrated on a small scale it should be possible to build full versions with reasonably low technical risk.

9. ACKNOWLEDGEMENTS

This work was funded in part by the Chinese Academy of Sciences under PIFI Project 2012T10002 and NSFC 11443009. Many thanks are also due to Xue Suijian, Feng Lu and Shen Zhixia for support and hospitality at the National Astronomical Observatories in Beijing.

8. REFERENCES

[1] P.Salinari, C. Del Vecchio, V. Bilotti: *A Study of an Adaptive Secondary Mirror,* Active and Adaptive optics: ESO Conference and Workshop Proceedings, Proceedings of the ICO-16 Edited by Fritz Merkle. Published by European Southern Observatory, Garching near Munich, p.247 (1994).

[2] Runa Briguglio, Roberto Biasi, Marco Xompero, Armando Riccardi, Mario Andrighettoni, Dietrich Pescoller, Gerald Angerer, Daniele Gallieni, Elise Vernet, Johann Kolb, Robin Arsenault, Pierre-Yves Madec: *The Deformable Secondary Mirror of VLT: final electro-mechanical and optical acceptance test results*, Proc. SPIE **9148**: Adaptive Optics Systems IV (2014).

[3] David R. Andersen, Jeff Stoesz, Simon Morris, Michael Lloyd-Hart, David Crampton, Tim Butterley, Brent Ellerbroek, Laurent Jolissaint, N. Mark Milton, Richard Myers, Kei Szeto, Andrei Tokovinin, Jean-Pierre Ve´ran, and Richard Wilson: *Performance Modeling of a Wide-Field Ground-Layer Adaptive Optics System,* PASP **118** 1574 (2006).

[4] M. Mark Colavita, Michael Shao, and David H. Staelin: *Atmospheric Phase Measurements with the Mark III Stellar Interferometer,* Appl. Opt. **26** 4016 (1987).

[5] Jean-Marc Conan, Gérard Rousset, and Pierre-Yves Madec: *Wave-front Temporal Spectra in High-Resolution Imaging Through Turbulence,* Journal of the Optical Society of America A **12**, 1559 (1995).

[6] D. G. MacMynowski, K. Vogiatzis, G. Z. Angeli, J. Fitzsimmons,and J. Nelson: *Wind Loads on Ground-Based Telescopes*, Appl. Opt. **45**, 7912 (2006).

[7] Douglas G. MacMynowskia, Carl Blaurockb, George Z. Angelic, and Konstantinos Vogiatzis: *Modeling Wind-Buffeting of the Thirty Meter Telescope*", Proc SPIE **6271**- 25, (2006).

[8] http://www.eso.org/sci/facilities/develop/ao/sys/dsm.html web site.

[9] J. Rakoczy, E. Montgomery, J. Lindner : *Recent Enhancements of the Phase Array Mirror Extendible Large Aperture (PAMELA) Telescope Testbed at MSFC*, Proc. SPIE 4004-61: Astronomical Telescopes and Instrumentation 2000, (2000).

[10] Edward Kibblewhite: *Building Bigger Telescopes from Smaller Segments,* SPIE Newsroom 23 (2010) DOI:10.1117/2.1201003.002645

[11] Leland Holloway, *Private Communication* (2006).

[12] A. Tokovinin: "Seeing Improvement with Ground-Layer Adaptive Optics" PASP, **116**, 941-951 (2004).

[13] Mark Chun, Richard Wilson, Remy Avila, Tim Butterley, Jose-Luis Aviles, Don Wier and Sam Benigni: *Mauna Kea Ground-Layer Characterization Campaign,* MNRAS. **394**, 1121(2009).

[14] Richard J. Sasiela: *Electromagnetic Wave Propagation in Turbulence,* Springer Publishing (1994).